The International Journal of Artificial Organs / Vol. 29 / no. 2, 2006 / pp. 251-260

Biomaterials

Multi-scale analysis of the Toraymyxin adsorption cartridge Part II: Computational fluid-dynamic study

G.B. FIORE, M. SONCINI, S. VESENTINI, A. PENATI, G. VISCONTI, A. REDAELLI

Department of Bioengineering, Politecnico di Milano, Milan - Italy

ABSTRACT: Extracorporeal endotoxin removal by means of the Toraymyxin device is based on the ability of polymyxin B to bind endotoxins with a high specificity. The endotoxins/polymyxin molecular interactions were computationally analyzed in a parallel work (Part I). In this paper we investigate with a multi-scale approach the phenomena involving blood and plasma fluid dynamics inside the device. The macro- and mesoscale phenomena were studied by means of 3D models using computational fluid dynamics. The flow behavior in the sorbent material was focused, modeling the sorbent as a homogeneous porous medium at the macroscale level, or accounting for the realistic geometry of its knitted fibers at the mesoscale level. A microscale model was then developed to analyze the behavior of endotoxin molecules subjected to the competition of flow drag and molecular attraction by fiber-grafted polymyxin B. The macroscale results showed that a very regular flow field develops in the sorbent, furthermore supplying the peak velocity to be input in the lower-scale model. The mesoscale analysis yielded the realistic range for wall shear stresses (WSSs) acting on fiber walls. With WSS values in the entire range, the results of the microscale analysis demonstrated that the capability of polymyxin B to capture endotoxin molecules from the flow extends at distances one order of magnitude greater than the characteristic distance of the stable intermolecular bond. We conclude that the use of an integrated, multi-scale analysis allows for a comprehensive understanding of the complex mechanisms involved in endotoxin sorption phenomena with immobilized polymyxin B. (Int J Artif Organs 2006; 29: 251-60)

KEY WORDS: Sepsis, Polymyxin B, Endotoxins, Multi-scale modeling, Computational fluid dynamics

INTRODUCTION

The need for effective and prompt remedies for patients affected by severe sepsis is becoming more and more urgent in the intensive care unit (ICU). Sepsis starts from a systemic inflammatory response and progresses rapidly into a generalized infection of the organism sustained by bacteremia, with concomitant single or multiple organ dysfunction or failure. This kind of clinical scenario leads patients to death (1) if not properly treated (2). Especially in critical conditions and in the presence of aged and/or immunodepressed subjects, sepsis is a major cause of mortality in the ICU (3, 4). In particular, in the United States, sepsis is the first cause of death in non-coronary ICUs (5), and the 11th cause of overall mortality (6). The incidence of sepsis has been increasing at an annual rate of 8.7%; the addressed causes are the aging of population, the common use of invasive procedures for the diagnosis/monitoring of critical patients, the upsurge of antibiotic-resistant organisms and the increased number of patients with compromised immune systems.

In recent years, studies have shown that early-goal therapies, as well as low-dose corticosteroids and activated Protein C, may significantly improve the survival rate of patients with sepsis. Nevertheless, the mortality remains dramatically high if we consider septic shock patients (2). Many efforts have been made in the last two decades to act on the primary trigger of the inflammatory process, i.e. the endotoxins (7). The idea started in the middle Seventies, when polymyxin B was discovered to be protective against endotoxin-induced hemodynamic shock (8-10). At the same time, however, polymyxin B was

0391-3988/251-10 $15.00/0

demonstrated to be extremely toxic for the kidney and for the central nervous system (10-13).

A number of antiendotoxin strategies have been proposed (e.g. monoclonal antibodies, antiendotoxin vaccines, inhibitors of endotoxin synthesis), however these have failed in demonstrating reproducible outcomes in septic subjects (7). A promising alternative approach involves treating blood extracorporeally by means of devices expressly dedicated to the selective removal of endotoxins.

The Toraymyxin device (Toray Medical Co., Tokyo, JP), has been on the market since 1994 (Japan), CE marked in 1998 and available in Europe since 2002. Its working principle is based on the known potential of polymyxin B to bind endotoxins. To avoid the side effects of polymyxin B, its molecule is grafted to an inert material (a knitted tissue of polypropylene and α-chloroacetamide-methylpolystyrene) with a covalent bond. In the Toraymyxin cartridge the patient's blood, withdrawn from a venous access, enters a central cylindrical blood distributor; it crosses the sorbent material (which is rolled up the central cylinder) in the radial direction; it is then routed into a collection chamber to be delivered to the device outlet and to the patient again. The passage through the porous sorbent region is meant to make blood lose its endotoxin component, thanks to the presence of the fiber-bound polymyxin B. Clinical studies (14-16) have demonstrated the effectiveness of the treatment with the Toraymyxin device. Its core functionality, however, is still debated: while some authors have reported about an important endotoxin removal effectiveness (17, 18), others did not observe any change in endotoxin levels (19), thus different effects underlying its documented clinical benefits have been hypothesized.

In this work, a multi-scale fluid-dynamic analysis of the Toraymyxin cartridge during operation has been carried out. The work's layout was arranged as follows. In step I, a macroscale model was developed with computational fluid dynamics (CFD) methods, to characterize the whole device in terms of its overall fluid-dynamic variables: pressures and velocities are calculated in the whole flow domain, part of which is occupied by the sorbent material, modeled as a continuum. In step II, a mesoscale model was defined: realistic geometrical models of the knitted fiber structure were constructed and CFD simulations were run with input fluid velocities equal to the worst-case data calculated at step I. Finally at step III, a microscale model was set up to analyze the behavior of endotoxin molecules, modeled as particles dragged by the flow field, in the presence of a fiber surface where polymyxin binding sites are present. The model at this scale not only uses data from the upper level model (the shear stresses calculated at step II) but also uses force expressions obtained in a parallel work dealing with the endotoxin/polymyxin molecular interactions, described in a companion paper (Part I). In the microscale model the competition between dragging and binding forces is described, therefore its output information shed light about the capability of the sorbent material to capture endotoxin molecules in the Toraymyxin device.

MATERIALS AND METHODS

The macro- and mesoscale models were developed using commercial software packages from Fluent Inc. (Lebanon, NH, USA); in particular, Gambit 2.1 was used to build 3D geometrical models and for volume meshing; Fluent 6.1 was used to set up and run CFD simulations with the finite-volume technique.

The microscale model was developed using the commercial package Simnon (SSPA, Göteborg, Sweden) to solve nonlinear differential equations numerically with the Runge-Kutta 4/5 method.

Macroscale model: Overall fluid dynamics within the Toraymyxin cartridge

The 3D geometrical model of the flow path inside the Toraymyxin device (Fig. 1) was built starting from technical drawings provided by the manufacturer. The shape has a double symmetry with respect to planes intersecting at the device's axis, which allowed us to model only one fourth of the real shape, thus notably reducing the computational complexity. The volume was meshed with 1,560,000 tetrahedral cells.

Macroscale CFD simulations were run with the following general assumptions: laminar flows, Newtonian, homogeneous, incompressible fluids. No-slip boundary conditions were applied at the walls.

The volume region occupied by the sorbent material was modeled as a permeable porous medium behaving according to the linear Darcy's law: $\nabla p = -\frac{\mu}{\alpha}\mathbf{v}$, where ∇p is pressure gradient, $\mathbf{v}$ is the so-called apparent fluid velocity vector, μ is fluid viscosity, α is the porous medium's permeability. An iterative procedure was needed

to determine the appropriate value for α. The available experimental data to be matched (flow rate-pressure drop relationship obtained by the manufacturer) provided an inlet-to-outlet pressure drop range of 15-18 mmHg at an inlet water flow rate of 100 ml/min at room temperature. A number of preliminary simulations were then run, setting density $\rho = 1000$ kg m^{-3} and viscosity $\mu = 1 \cdot 10^{-3}$ kg m^{-1} s^{-1} (as for water at 20°C) and imposing the flow rate while changing α between simulations. The matching values for α resulted in the range $(5.90\text{-}7.05) \cdot 10^{11}$ m^{-2}.

Blood simulations were performed with α values set at both limits of the matched range, in order to check the results' sensitivity to this parameter. The normal working conditions for the Toraymyxin cartridge were mimicked, involving a 100-ml/min inlet blood flow rate at 37°C. A density $\rho = 1060$ kg m^{-3} was set for blood. As for viscosity, a sensitivity analysis was performed by setting blood viscosity at values in the range $\mu = (2.7\text{-}4.0) \cdot 10^{-3}$ kg m^{-1} s^{-1} (20). Since one aim of these simulations was the estimation of the worst-case (or, peak) velocity in the sorbent region, to be used in the subsequent mesoscale model, post-processing was oriented at evaluating the fluid velocity distribution in the porous flow field.

Mesoscale model: Fluid dynamics across the sorbent tissue

The mesoscale model was built at a scale involving characteristic dimensions of order 1 mm. At this scale, the sorbent material is no longer describable as a homogeneous medium, rather the real geometrical features of the knitted fibers have to be taken into account. To this purpose, first a realistic 3D model of a single texture layer was developed based on optic microscopy (Fig. 2a). In building this model, the geometry was slightly simplified by maintaining the knitted fibers in plane and considering fibers as solid impermeable drums with a smooth surface. The resulting single-layer model is shown in Figure 2b. It was then necessary to construct multiple-layer clusters accounting for the random manner of how subsequent fiber layers superimpose during manufacturing. Clusters were built superimposing four knitted layers. Cluster A was built with the fibers belonging to different layers perfectly aligned, whereas clusters B and C have differently translated fiber layers. The volumes pertaining to the fluid were then obtained subtracting each fiber cluster from a 3.6 mm x 4.5 mm x 25 mm parallelepiped, yielding the geometrical models A, B and C shown in Figure 3. The

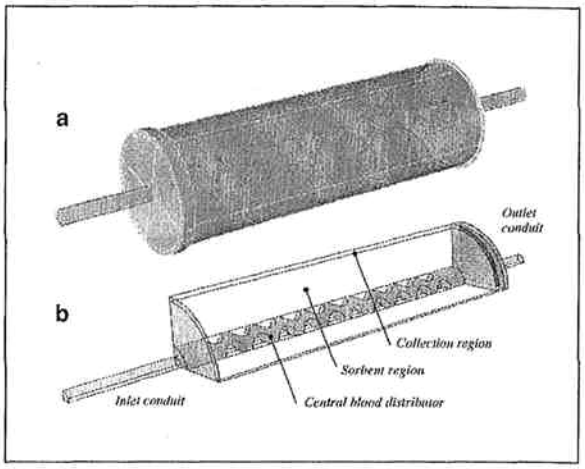

Fig. 1 - *Macroscale model.* **(a)** *3D sketch and* **(b)** *geometrical model of the Toraymyxin filter: one fourth of the overall geometry is modeled thanks to the cartridge's symmetry.*

largest edge was provided in the main flow direction in order to apply the velocity inlet boundary condition on a plane far enough from the fibers. Models were meshed with around 230,000 tetrahedral cells each.

Mesoscale CFD simulations were run assuming laminar flow of a Newtonian, homogeneous, incompressible fluid of density $\rho = 1060$ kg m^{-3} and viscosity $\mu = 4 \cdot 10^{-3}$ kg m^{-1} s^{-1}. The no-slip boundary condition was applied at the fiber surfaces, while a periodic boundary condition was used on the faces of the parallelepiped which are parallel to the main flow direction. The inlet velocity was set equal to the largest value obtained in the macroscale simulations within the sorbent region. Post-processing of the mesoscale simulations was aimed at estimating wall shear stresses (WSSs) to be used for the sake of comparison in the subsequent microscale model.

Microscale model: Study of the flow dragging and fiber binding of endotoxin molecules

The microscale model was built considering submicrometric characteristic dimensions, at which it is possible to describe the competition between the molecular interaction forces, as calculated with molecular mechanics methods (Part I), and the forces due to flow drag.

At this scale level, it was considered that a single fiber surface could be approximated as planar, and that the local fluid dynamic situation in the adjacent fluid layer is

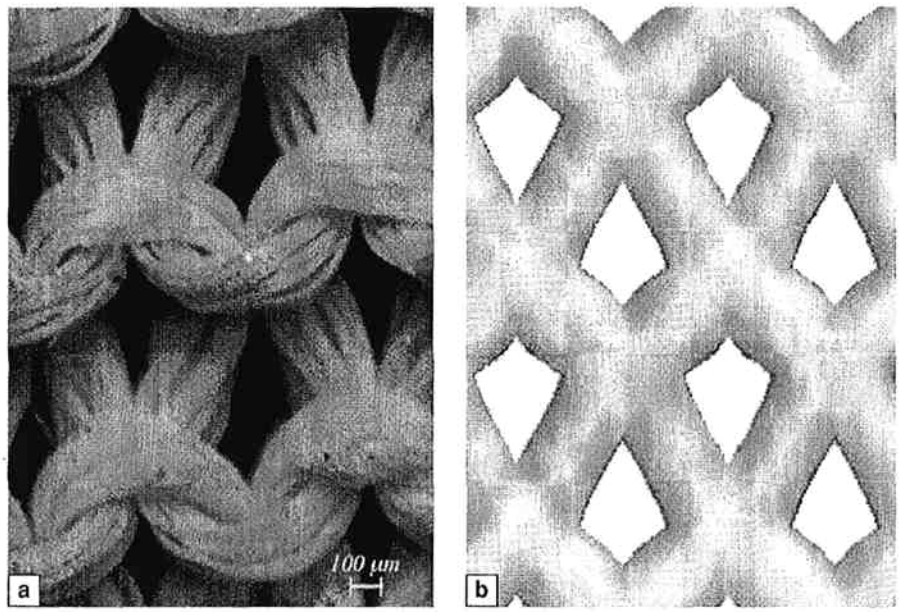

Fig. 2 - *Mesoscale model.* **(a)** *The structure of the knitted sorbent tissue, as displayed with optic microscopy.* **(b)** *The in-plane 3D geometry used in the mesoscale analysis to model the tissue.*

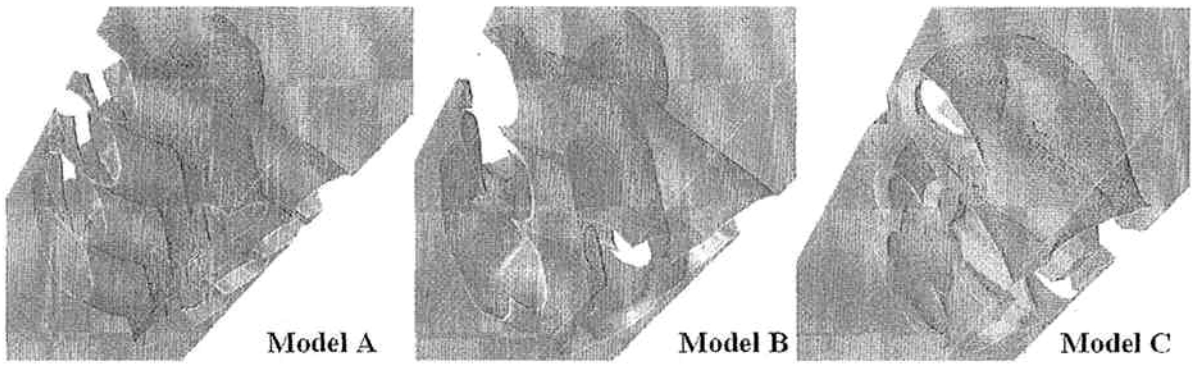

Fig. 3 - *Mesoscale model. 3D models of fluid volumes, obtained by subtracting fiber clusters from parallelepiped volumes.*

reduced to the case of simple shear flow against a flat solid surface. A Cartesian 2D domain was thus considered, with axis *z* coincident with the fiber surface and oriented as the direction of the flow in the adjacent fluid, and axis *y* measuring the distance from the surface. In the fluid, a velocity profile increasing linearly with *y* was applied to represent shear flow. This velocity profile was assumed to be undisturbed in the presence of moving particles. The slope of the profile (i.e., the shear rate) is related to the applied WSS through fluid viscosity. The rheologic characteristics of plasma were used in this case (ρ = 1035 kg m^{-3} and μ = 1.6 • 10^{-3} kg m^{-1} s^{-1}), since the scale of the analyzed phenomena is small enough that the behavior in the sole plasma sublayer can be isolated.

Endotoxin molecules dragged by the flow were represented as buoyant spherical particles, whose dimensions were determined based on the so-called van der Waals volume occupied by the molecules. Referring to (Part I), the complete endotoxin structure (S-LPS, equivalent radius r_{eq} = 1.56 nm) and the minimum structure that is known to display an endotoxin activity (ReLPS, r_{eq} = 1.07 nm) were considered.

Endotoxin molecules were assumed to obey the Stokes' law when dragged by the flow:

$$\mathbf{F}_d = 6 \pi \mu r_{eq} (\mathbf{v} - \mathbf{v}_p)$$

Where $\mathbf{F}_d$ is the drag force vector and $\mathbf{v} - \mathbf{v}_p$ is the difference between the fluid velocity vector and the particle's velocity vector.

A single polymyxin B molecule was located on the fiber wall, at coordinate z = 15 nm. Its binding site was located at a distance y = 2.6 nm from the wall, in consideration of the overall molecule length. The endotoxin-polymyxin molecular interaction was modeled as a central force, applied to the endotoxin particle, pointing towards the polymyxin's binding site. The force is expressed as a function of the endotoxin-to-polymyxin intermolecular distance r (i.e. the distance of their centers of mass) according to the Lennard-Jones model:

$$F_{LJ} = - 24 \varepsilon \left[2 \frac{\sigma^{12}}{r^{13}} - \frac{\sigma^6}{r^7} \right]$$

(positive values are attraction forces), where σ and ε are the parameters of the corresponding expression for interaction energy. Based on the results of molecular-mechanics simulations (Part I), and choosing the values yielding the smallest peak attraction forces, σ = 0.63 nm and ε = 274 kJ/mol were used for the S-LPS-to-polymyxin interaction, and σ = 0.58 nm and ε = 196 kJ/mol were used for the ReLPS-to-polymyxin interaction.

Simulations were run with five different WSS values in the interesting range identified by the mesoscale results. In the simulations pertaining to each WSS value, the domain was seeded with one particle per simulation and the trajectory of the particle's center of mass was traced. Each particle was initially placed at $z = 0$ and at different y, with an initial velocity vector set equal to that of the fluid at the same y.

RESULTS

Macroscale model

Simulations run with parameters mimicking the normal working conditions for the Toraymyxin cartridge show that the velocity distribution within the volume region occupied by the sorbent is quite uniform. As an example, a velocity map is shown in Figure 4: peak velocities reaching values around 8 mm/s take place in the distributor region only, particularly where the flow changes in direction. But, as soon as the flow impacts the porous region, a notable dampening effect takes place and, at the porous region's outlet surface, velocity differences are no longer perceptible. Moreover, Figure 5 shows that the fluid follows radially-oriented pathlines when traveling through the sorbent, pointing out that a very regular and undisturbed fluid-dynamic pattern takes place in this region.

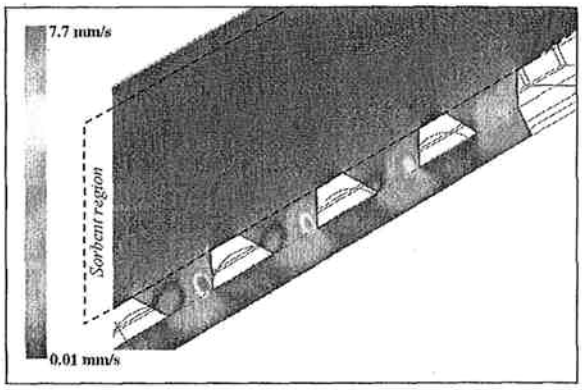

Fig. 4 - *Macroscale model. The fluid velocity map on a plane intersecting the sorbent region shows that the highest velocity takes place in the distribution channels, out of the sorbent. Peak velocity in the sorbent region takes place immediately beyond the impact surface to the sorbent itself.*

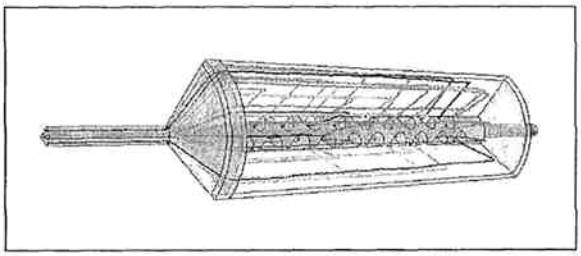

Fig. 5 - *Macroscale model. Fluid pathlines show a very regular flow within the sorbent region.*

The peak velocity in the sorbent region, i.e. the worst-case velocity value that serves as an input parameter for the subsequent mesoscale simulations, is located immediately below the impact surface. Its value showed to be quite insensitive to the values used for permeability α and fluid viscosity μ as well as to the axial position: considering all the performed simulations, the peak velocity ranged from 0.354-0.356 mm/s.

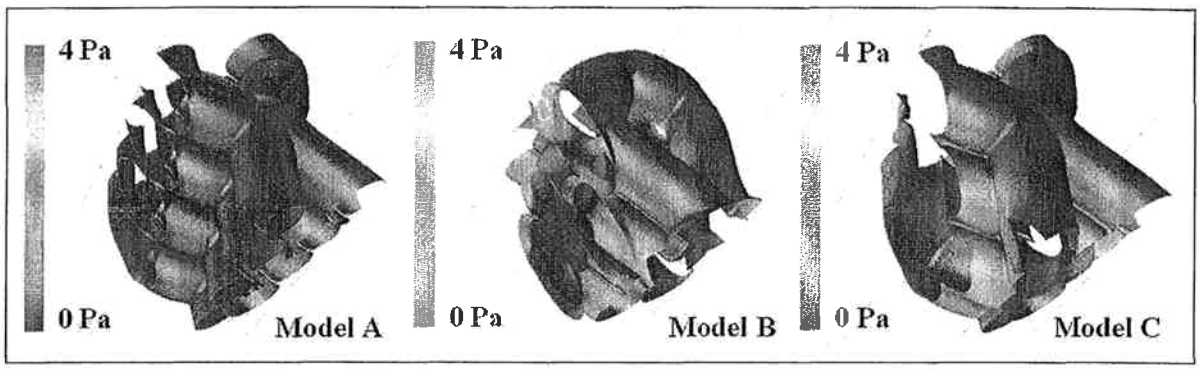

Fig. 6 - *Mesoscale model. Wall shear stress (WSS) maps at the fiber walls: WSS is quite homogeneous for model A; models B and C show uneven WSS patterns.*

Mesoscale model

The results of the mesoscale-model simulations have been analyzed in terms of the WSS values calculated at the fibers' surfaces. Figure 6 compares the resulting WSS patterns for the three different geometrical models as WSS maps. For model A the WSS distribution is quite homogenous in the whole region as a result of the perfect alignment of the fibers pertaining to different fiber layers. Much more uneven WSS patterns are found for models B and C; for these models, the largest WSS values were found on the walls of the first fiber layer encountered by the flow.

Each geometrical model contained a number of wall elements ranging from 16,700 to 25,000, therefore the resulting WSS values were treated as a statistical population. Figure 7 shows a histogram distribution of WSS values extracted from the simulation pertaining to model B. The distribution shows a large spread on low values, with a median of 0.140 Pa (1.40 dyne/cm^2) and a 90th percentile of 1.04 Pa (10.4 dyne/cm^2). The tail of the distribution extends up to a maximal value of 4.91 Pa (49 dyne/cm^2), however the frequency distribution approaches zero soon when increasing WSS. This analysis was applied to all three models and the results were collected in Table I. The worse WSS distributions were found for Models B and C, which will be used as reference WSS cases for the microscale model.

Microscale model

The calculated trajectories for an endotoxin particle, as simulated in the microscale model, depends upon the initial particle distance from the fiber wall and WSS. At a given WSS, there exists a threshold value y_T for the initial distance at which the particle is seeded: particles starting their motion at $y < y_T$ are captured by the polymyxin molecule; particles starting at $y > y_T$ are dragged away by the flow. Figure 8 represents an example plot of the trajectories of ReLPS particles seeded at different heights (y = 4-18 nm) at WSS = 1 Pa, approximately equaling the 90th percentile WSS resulting from the mesoscale models B and C. The plot shows that particles seeded in the vicinity of the threshold distance y_T (= 12.44 nm in this case) follow trajectories that may diverge dramatically, as a result of the competition of molecular forces and drag forces.

Simulations were carried out for the S-LPS and ReLPS molecules at each WSS (range: 0.06-5 Pa) to determine y_T with a precision of 0.02 nm. Results are reported in Figure 9, where the threshold heights are plotted versus the applied WSS values, yielding almost linear behaviors in a semi-logarithmic plot. Each of the lines in Figure 9 splits the y - WSS plane into two regions: the region below the line (binding region) identifies the conditions for the endotoxin particle to be captured and bound to the polymyxin molecule, whereas the region above the line (non-binding region) identifies the conditions for the drag

TABLE I - RELEVANT WSS VALUES OBTAINED IN THE MESOSCALE MODELS

Model	# of wall elements	Median [Pa]	90th percentile [Pa]	Max. value [Pa]
A	25,066	0.0657	0.364	0.824
B	21,423	0.140	1.04	4.91
C	16,756	0.154	0.935	2.89

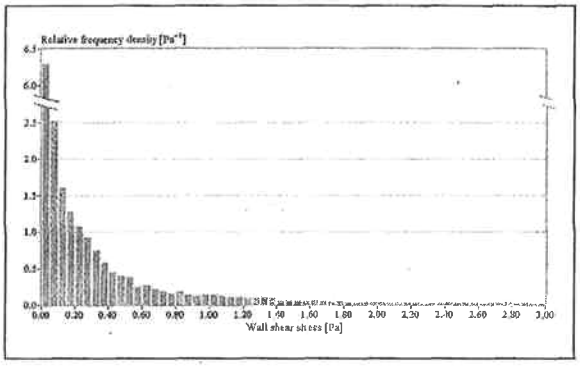

Fig. 7 - *Mesoscale model. Histogram distribution of WSS in model B: the distribution is polarized onto low WSS values; the tail extends up to 4.91 Pa (not shown).*

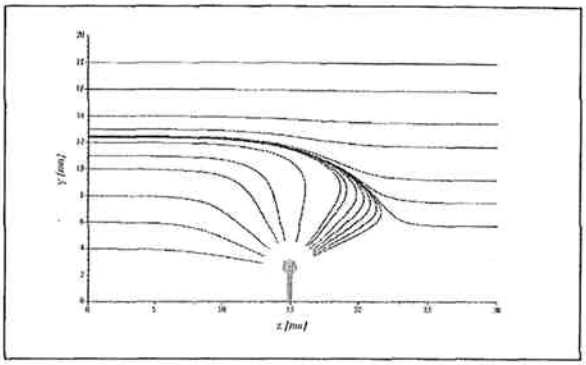

Fig. 8 - *Microscale model. Trajectories of the center of mass of endotoxin particles in the (z, y) domain, with axis z coincident with the fiber surface. A single polymyxin B molecule is located at z = 15 nm, with its binding site at y = 2.6 nm. Trajectories of distinct particles starting their motion at different y are shown.*

force to prevail. The behaviors of the S-LPS and Re LPS molecules do not differ much: in fact, even if the S-LPS particle is attracted by polymyxin with a greater force, S-LPS is bigger than ReLPS, therefore also experiences greater drag forces. In Figure 9, the relevant WSS values from the mesoscale analyses (referred to models B and C) are reported for comparison.

DISCUSSION

The aptitude of fiber-grafted polymyxin B to bind endotoxins with a high specificity is the basic working principle that the Toraymyxin device relies on. The molecular interaction between endotoxins and polymyxin B, for which there was a dedicated analysis in Part I, involves a stable bond, attained thanks to hydrophobic interactions, for intermolecular distances up to 1 nm, whereas, for further distances, the interaction is mainly electrostatic, yielding forces of an extremely smaller magnitude. In this work, we focused on the phenomena involving blood and plasma fluid dynamics, starting from a macroscale analysis, then zooming down to the mesoscale, and finally to the microscale level, where fluid-dynamic related forces and molecular forces interact. At each scale level, quantitative information was passed to the lower-scale level as input data: as a general approach, this was performed pessimistically (i.e., choosing the worst case) to avoid any unwanted bias. Our analysis demonstrated that, for the whole range of realistic shear stresses interesting the fluid layer next to the wall, the

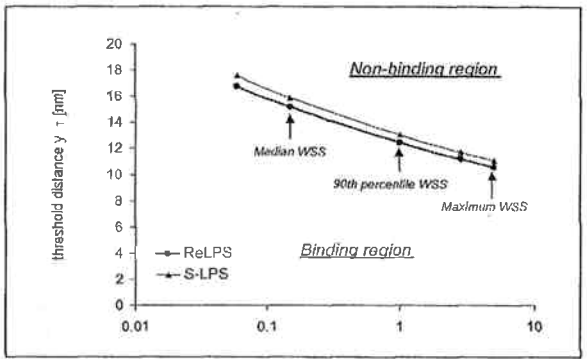

Fig. 9 - *Microscale model. Relationship between the threshold distance and the applied WSS, for the S-LPS and ReLPS molecules. WSS values are plotted with a logarithmic scale. Arrows indicate the relevant WSS emerging from the mesoscale analysis (models B and C). Each line splits the plane in two regions: the binding region, and the non-binding region.*

fiber-grafted polymyxin B is able to capture endotoxin molecules up to distances far beyond the short-range interval that is characteristic of the ultimate stable intermolecular bond.

In the macroscale model, modeling assumptions were applied according to the common practice of CFD analyses dealing with extracorporeal blood devices (21). In particular, the choice of treating the sorbent region as a linear porous medium was justified by the order of magnitude of its overall pressure drop, derived from experimental data (~10 mmHg). From simple preliminary calculations, in the sorbent region a velocity of order 1 mm/s could be expected, at worst, for blood; the kinetic

pressure associated to such a velocity (~10^{-5} mmHg) was so small that nonlinear effects could be safely neglected. This, in its turn, allowed to characterize the sorbent medium with a single parameter (its permeability, α) whose value was assigned through an iterative procedure matching the model-calculated pressure drop with the known experimental data range. In order to verify the model's reliability, blood simulations were then conducted with α values pertaining to the whole range and, convincingly, the simulated velocity field proved to be insensitive to it. An additional indetermination existed concerning blood viscosity, for which a wide range is reported in the literature (20); again, the sensitivity of the velocity field to this parameter was tested and was verified to be quite irrelevant.

Concerning the results of the macroscale model, their primary goal was to supply a worst-case input for the subsequent mesoscale model, i.e. the peak velocity in the sorbent region (0.355 mm/s), that was found to occur immediately beyond the impact surface with the sorbent itself. Most of the volume pertaining to the sorbent, however, experiences fluid velocities much below the peak value (for instance, at the outlet surface the velocity is 0.07 mm/s). The uniformity of the velocity field (Fig. 4) and the straightness of pathlines (Fig. 5) show that the available sorbent volume is well exploited by the blood flow, confirming previous experimental observations (22).

Geometrical modeling at the mesoscale level involved building realistic 3D models of the sorbent material. Indeed, the scale of this analysis was established so as to allow access to the desired output information, i.e. the values for the shear stress acting on fiber walls, to be passed to the lower-scale analysis. The geometrical simplifications applied (solid knitted fibers kept in plane) were motivated by the necessity of facilitating the construction of good quality meshes, with a limited number of elements, still catching the main geometrical features of the tissue texture (Fig. 2). As in the macroscale case, the Newtonian model was used for blood according to the following considerations. It is well known that blood can be conveniently modeled as Newtonian (i) with shear rates > 200 s^{-1} and (ii) in macroscopic flow (23). The case studied meets condition (i), however approaches the limit of validity for condition (ii), because the characteristic dimensions of the flow paths through the knitted fibers are of order 100 μm (one order of magnitude greater than the average red blood cell diameter). Nonetheless, the Newtonian assumption was held valid in our model, because the complex geometrical paths through the knitted tissue, even with laminar flow, are expected to cause blood pathlines to be quite tortuous. In a condition of frequently changing velocity direction, a considerable mixing is expected, therefore the reasons that bring blood out of the Newtonian behavior (namely, the axial gathering of red cells and the formation of rouleaux), are likely avoided. We cannot, however, evaluate to what extent this assumption may have influenced the obtained results, and are aware that this issue deserves further attention.

At the microscale level, finally, our aim was that of investigating the basic sorption phenomena that blood-contained endotoxin molecules undergo when the blood stream comes in contact with the sorbent material. The analysis was quite simplified with respect to reality, however it is also thanks to simplicity that the developed model has the power of catching the essential characters of the phenomena. The steric complexity of molecules was not considered except for molecule dimensions (equivalent radii of endotoxin molecules, modeled as buoyant spherical particles) and for proper locating of the polymyxin binding site 2.6 nm far from the underlying fiber surface. Endotoxin particles were supposed to respond to two contending forces: those due to molecular interactions and those due to fluid drag. Modeling of molecular forces was done using the Lennard-Jones expression, according to the quantitative results of our dedicated study (Part I), which also accounts for the presence of a water-like environment in determining interactions; for caution, among the (σ, ε) parameter pairs available for each case, the one yielding the weakest force was chosen. Drag forces were expressed through the classical Stokes' law; in this, the main modeling assumption was that of considering particles immersed in a continuum fluid: this is supported by observing that the dimension of the considered endotoxin molecules is 1 order of magnitude greater than that of water molecules. What has been completely ignored is the possibility of endotoxin molecules to be subject to Brownian motions. This must have caused underestimation of the capturing potential by polymyxin B. In fact, Brownian motions would cause trajectories to erratically deviate from the ones calculated with our model. Now, whereas drag forces are linear with the particle distance from the wall, the interaction force is strongly nonlinear. In the long-range intermolecular distance (> 1 nm), bringing molecules closer causes an

increase in the attraction force which well exceeds the corresponding decrease obtained when molecules are parted. Inclusion of Brownian motions would therefore add a stochastic term whose net result would be in favor of molecular attraction.

The potential for seizing endotoxins by a single polymyxin B molecule was expressed as the maximum distance above the surface allowing the binding of a traveling endotoxin molecule. It is quite interesting to observe that, with WSS values spanning two orders of magnitude (0.06 to 5 Pa), such threshold distance keeps between 10-20 nm, which is a far range for endotoxin-polymyxin molecular interaction (Part I). This, *per se*, is an indication of sorption potential: it has to be considered that at these distances the molecular attraction force is 8-10 orders of magnitude lower than the maximum attraction force, which takes place in the short-range intermolecular distances (of the order of 1 nm). One also has to consider that the one-to-one molecule coupling considered here is quite unrealistic: based on data supplied by the manufacturer, the average surface concentration of fiber-grafted polymyxin B molecules is 0.25 molecules/nm^2, which means, in a 2D domain, an average linear concentration of one molecule every two nanometers. An endotoxin particle traveling above the surface would therefore experience the attraction from an entire surface field of rooted polymyxin molecules working synergistically; for instance, in the 30-nm-long domain of Figure 8, fifteen polymyxin binding sites should be considered on the bottom line. Again, our prediction must have underestimated the real adsorption potential of the surface.

With all the above considerations from each observation scale in mind, one can take a possible picture of the overall mechanisms influencing Toraymyxin's antiendotoxin effect, as follows. Close to the surface of fibers, even at relatively high WSSs, an endotoxin-free plasma layer is likely to form quite immediately. Above a certain distance, of order tens of nanometers, endotoxin concentration is not affected. As a consequence of this, a concentration gradient arises, promoting the diffusion of endotoxins towards the fiber wall. As far as the plasma sublayer is considered, thus, diffusion must be the major limiting factor for adsorption (we are leaving the problem of sorbent saturation out of consideration, of course). To compensate for this, a huge fiber area is needed, which explains why the overall blood-exposed surface in the Toraymyxin device is over 500 m^2 by design. As soon as we zoom out to a higher scale, however, convective effects start playing a role in the transport of endotoxins from the bulk of the fluid towards the fiber surface. Particularly, highly sheared blood flow may help, thanks to the microconvective effect applied by rotating erythrocytes or erythrocyte clusters (24); also, entangled blood pathways are expected to promote overall mixing much more than a flow with parallel streamlines would do. Indeed, even if path irregularity results in an increase in the overall WSS pattern, the analysis at the microscale has shown that this does not ingenerate dramatic changes in the local adsorbing behavior; using augmented WSSs as mixing enhancers therefore seems to be a safe choice. In this regard, as clearly pointed out in our mesoscale analysis, a misaligned superimposition of adjacent tissue layers must be preferred. This is, to some extent, also related to the fluid-dynamic behavior at a greater scale. Our macroscale results show that, under the hypothesis of a porous material with homogeneous characteristics, a broad utilization of the available sorbent is attained, with a regular blood flow well distributed in the whole flow field. Now, one possible way to obtain such a homogeneity would be superimposing the knitted tissue layers in a very regular manner, but in this case even the slightest inaccuracy would break symmetry and cause the formation of preferential blood paths, with a drop in the overall expected performance. A safer alternative, used in the Toraymyxin, is to follow the opposite strategy, that is laying the material in the most random manner, so to obtain an average homogeneity insensitive to layering imprecision, and additionally promoting the formation of lower-scale fluid dynamics enhancing blood mixing.

CONCLUSIONS

The use of extracorporeal blood purification for the treatment of sepsis is an interesting emerging technology with demonstrated clinical benefits. Its rationale, in the case of the Toraymyxin device, is centered on the removal of endotoxins from blood. The effectiveness of the Toraymyxin cartridge in abating the endotoxin content of an inlet fluid stream has been unequivocally proved *in vitro*, whereas contradictory results have been reported concerning the antiendotoxin effectiveness *in vivo*, whose quantification was much less straightforward. In this debate, we tackled the job of investigating through numerical tools the mechanisms that underlie the

endotoxin removal potentialities of the Toraymyxin device. Integrated knowledge and competencies were applied to a multi-scale approach ranging from the nanoscale, where the molecular interactions take place, to the macroscale, i.e. the scale at which the main blood stream is managed. An overall picture was obtained, displaying both the physics involved at each scale level and the mutual interactions of phenomena taking place ad different levels. Even if our results, at this stage, cannot be directly compared with experimental data, we believe we have made a decisive step towards a comprehensive understanding of the matter.

ACKNOWLEDGEMENTS

The authors are grateful to Dr. Gualtiero Guadagni (Estor SpA, Milan, Italy) and Dr. Hisata Shoji (Toray Medical Inc., Tokyo, Japan) for assistance with the manuscript and for supplying materials, technical drawings and design details.

Address for correspondence:
Ing. Gianfranco B. Fiore, PhD
Department of Bioengineering
Politecnico di Milano
Piazza Leonardo da Vinci, 32
20133 Milano, Italy
e-mail: gianfranco.fiore@polimi.it

REFERENCES

1. Bone RC. Gram-negative sepsis: A dilemma of modern medicine. Clin Microbiol Rev 1993; 6: 57-68.
2. Bernard GR, Vincent JL, Laterre PF, LaRosa SP, Dhainaut JF, Lopez-Rodriguez A, Steingrub JS, Garber GE, Helterbrand JD, Ely EW, Fisher CJ Jr. Recombinant human protein C worldwide evaluation in severe sepsis (PROWESS) study group. Efficacy and safety of recombinant human activated protein C for severe sepsis. N Engl J Med 2001; 344: 699-709.
3. Friedman G, Silva E, Vincent JL. Has the mortality of septic shock changed with time? Crit Care Med 1998; 26: 2078-86.
4. Balk RA. Pathogenesis and management of multiple organ dysfunction or failure in severe sepsis and septic shock. Crit Care Clin 2000; 16: 337-52.
5. Martin GS, Mannino DM, Eaton S, Moss M. The epidemiology of sepsis in the United States from 1979 through 2000. N Engl J Med 2003; 348: 1546-54.
6. Murphy SL. Deaths: Final data for 1998. Natl Vital Stat Rep 2000; 48: 1-105.
7. Opal SM, Gluck T. Endotoxin as a drug target. Crit Care Med 2003; 31 (suppl): S57-64.
8. Palmer JD, Rifkind D. Neutralization of the hemodynamic effects of endotoxin by polymyxin B. Surg Gynecol Obstet 1974; 138: 755-9.
9. From AH, Fong JS, Good RA. Polymyxin B sulfate modification of bacterial endotoxin: Effects on the development of endotoxin shock in dogs. Infect Immun 1979; 23: 660-4.
10. Baldwin G, Alpert G, Caputo GL, Baskin M, Parsonnet J, Gillis ZA, Thompson C, Siber GR, Fleisher GR. Effect of polymyxin B on experimental shock from meningococcal and *Escherichia coli* endotoxins. J Infect Dis 1991; 164: 542-9.
11. Cooperstock MS. Inactivation of endotoxin by polymyxin B. Antimicrob Agents Chemother 1974; 6: 422-5.
12. Danner RL, Joiner KA, Rubin M, Patterson WH, Johnson N, Ayers KM, Parrillo JE. Purification, toxicity, and antiendotoxin activity of polymyxin B nonapeptide. Antimicrob Agents Chemother 1989; 33: 1428-34.
13. Wheeler AP. Bacterial peritonitis: Innovative experimental treatment. Crit Care Med 1999; 27: 1055-6.
14. Suzuki H, Nemoto H, Nakamoto H, Okada H, Sugahara S, Kanno Y, Moriwaki K. Continuous hemodiafiltration with polymyxin-B immobilized fiber is effective in patients with sepsis syndrome and acute renal failure. Ther Apher 2002; 6: 234-40.
15. Shoji H. Extracorporeal endotoxin removal for the treatment of sepsis: Endotoxin adsorbtion cartridge (Toraymyxin). Ther Apher Dial 2003; 7: 108-14.
16. Kushi H, Miki T, Okamaoto K, Nakahara J, Saito T, Tanjoh K. Early hemoperfusion with an immobilized polymyxin B fiber column eliminates humoral mediators and improves pulmonary oxygenation. Crit Care 2005; 9: R653-61.
17. Nakamura T, Matsuda T, Suzuki Y, Shoji H, Koide H. Polymyxin B-immobilized fiber hemoperfusion in patients with sepsis. Dial Transplant 2003; 32: 602-7.
18. Nemoto H, Nakamoto H, Okada H, Sugahara S, Moriwaki K, Arai M, Kanno Y, Suzuki H. Newly developed immobilized polymyxin B fibers improve the survival of patients with sepsis. Blood Purif 2001; 19, 361-9.
19. Vincent JL, Laterre PF, Cohen J, Burchardi H, Bruining H, Lerma FA, Wittebole X, De Backer D, Brett S, Marzo D, Nakamura H, John S. A pilot-controlled study of a polymyxin B-immobilized hemoperfusion cartridge in patients with severe sepsis secondary to intra-abdominal infection. Shock 2005; 23: 400-5.
20. Wells R. Syndromes of hyperviscosity. N Engl J Med 1970; 283: 183-6.
21. Fiore GB, Redaelli A, Guadagni G, Inzoli F, Fumero R. Development of a new disposable pulsatile pump for cardiopulmonary bypass: CFD design and *in vitro* tests. ASAIO J 2002; 48: 260-7.
22. Ronco C, Brendolan A, Scabardi M, Ronco F, Nakamura H. Blood flow distribution in a polymyxin coated fibrous bed for endotoxin removal. Effect of a new blood path design. Int J Artif Organs 2001; 24: 167-72.
23. Pennati G, Fiore GB, Migliavacca F, Lagana' K, Dubini G, Fumero R. *In vitro* steady-flow analysis of systemic-to-pulmonary shunt haemodynamics. J Biomech 2001; 34: 23-30.
24. Wang NL, Keller KH. Augmented transport of extracellular solutes in concentrated erythrocyte suspensions in Couette flow. J Colloid Interface Sci 1985; 103: 210-25.